Anisotropy and Mechanical Characteristics of Ultra-High Performance Concrete and Its Interpenetrating Phase Composite With Triply Periodic Minimal Surface Architectures

Ba-Anh Le, Bao-Viet Tran, Thai-Son Vu, Quoc-Bao Nguyen, Hoang-Quan Nguyen, Xavier Chateau

ANISOTROPY AND MECHANICAL CHARACTERISTICS OF ULTRA-HIGH PERFORMANCE CONCRETE AND ITS INTERPENETRATING PHASE COMPOSITE WITH TRIPLY PERIODIC MINIMAL SURFACE ARCHITECTURES

Ba-Anh LE [1], Bao-Viet TRAN [1], Thai-Son VU [2 *], Quoc-Bao NGUYEN [2], Hoang-Quan NGUYEN [1] and Xavier CHATEAU [3]

1 : University of Transport and Communications, 3 Cau Giay, Lang Thuong, Dong Da, Ha Noi, Viet Nam.
2 : Department of Bridge and Road Engineering, Hanoi University of Civil Engineering, Ha Noi, Viet Nam.
3 : Navier, Ecole des Ponts, Univ Gustave Eiffel, CNRS, Marne-la-Vallée, France.
* Corresponding author: sonvt2@huce.edu.vn

ABSTRACT

This work numerically explores the anisotropy, impact phase wave propagation, buckling resistance, and natural vibration of ultra-high performance concrete (UHPC) and UHPC-steel interpenetrating phase composite (IPC) with triply periodic minimal surfaces (TPMSs), including sheet and solid Gyroid, Primitive, Diamond, and the Schoen I-graph-wrapped package (I-WP). The experiment is conducted to verify the accuracy of the numerical model in terms of Young's modulus of polylactic acid (PLA)-based TPMS lattices and PLA-cement IPCs with TPMS cores, with the highest percent difference of 15% found for IPCs and 17% found for lattice. The results indicate that UHPC material with sheet Gyroid exhibits the least extreme anisotropy in response to the varying orientation among other lattices regardless of the change of solid density, making it the ideal candidate for construction materials. Interestingly, compared to UHPC-based TPMS lattice, IPCs possess a much smaller anisotropy and exhibit almost isotropy regardless the variation of solid density and TPMS topology, offering a free selection of TPMS type to fabricate IPCs without much care of anisotropy. The phase wave velocity and buckling resistance of UHPC- and IPC-based beams with TPMSs nonlinearly decrease with a drop of TPMS solid density, but it is the almost linear pattern for the case of natural vibration frequency. UHPC material and IPC with sheet Gyroid lattice are found to possess the lowest phase wave velocity and exhibit the least anisotropy of wave propagation, showing it as an ideal candidate for UHPC material to suppress the destructive energy induced by the external impact.

Keywords: ultra-high performance concrete; triply periodic minimal surface; numerical model; anisotropy; impact phase wave propagation; buckling resistance; free vibration.

1. INTRODUCTION

Owing to extreme natural and artificial activities, including earthquakes, manmade impacts, explosions, and the like, together with the increasing size of civil engineering structures, like buildings, bridges, etc. It necessarily requires building materials to have good resistance to such events while maintaining high durability and strength. Traditional concrete materials are susceptible to the abovementioned activities due to their intrinsic brittleness and low tensile strength[1-5]. Thus, to enhance structure strength in front of such activities, UHPC has been introduced, by mixing an appropriate ratio of fiber, water, limestone, fine sand, portal cement, and reactive powder, resulting in excellent strength (>150 MPa in compression), excellent flexibility, self-healing ability[6], corrosion resistance[7], impact resistance, good resistance to the wide range of extreme climate conditions [8,9], reduction of service cycles, and the enhanced durability and longevity under such harsh conditions[10], making it as one of the ultimate options for constructing the civil engineering structures. Due to these outstanding properties, UHPC has been recently used in innovative civil engineering applications, such as bridges [11], concrete structures exposed to extreme environments[12], and ultra-high-rise buildings[13], structural integrity enhancement[14], and modern shading panels[15]. Besides, cutting-edge research was being undertaken to further investigate and enhance the mechanical properties of UHPCs. Indeed, Yao et al.[1] investigated the impact behaviour of UHPC by conducting several flexural impact tests and reported that the flexural impact strength, ductility, and energy absorption capacity of the UHPC specimens rise with increasing input energy of flexural impact. Furthermore, the UHPC samples demonstrated high impact resistance and ductility via various cracking behaviors. A good impact resistance of steel-reinforced UHPC is also experimentally and numerically found in the research work[16]. Xu et al. [17] experimentally and numerically investigated the blast resistance of steel tubes filled with UHPC. The authors reported that the tube filled with UHPC performed better blast-resistant compared with that of conventional concrete with identical earthquake intensity. Mirdan et al. [18] conducted experimental research to investigate the stiffness improvement and crack resistance for the conventional concrete beam by incorporating UHPC layers. The authors found that the inclusion of UHPC layers at the tensile side of the concrete beams significantly increased their stiffness (20–132 %) and delayed the crack onset. In similar research[19], the concrete beam embedded by the UHPC layer is experimentally reported to suppress effectively the cracking of the beam, making the crack propagate slower in the concrete beam upon the increasing load. The influence of reinforcing ratio and fiber volume on the flexural hardening behavior of steel-reinforced UHPC beams is also experimentally reported in detail in the work[20]. Yu et al. [21] investigated the behaviour of steel-combined UHPC under the near-field blast load. the authors reported that the combination could significantly enhance the blast resistance of composite panels. The mechanical behaviour of the fire-damaged UHPC subjected to the coupled axial static and impact loading was investigated by

Liu et al. [22]. The results indicated that UHPC under axial static compression performs better the dynamic mechanical properties such as compressive strength and elastic modulus than without axial static compression.

Among nature-inspired architected porous metamaterials, TPMS is renowned for its outstanding mechanical and physical properties, including possessing the ultrahigh surface area-to-volume ratio, a high strength-to-weight ratio, mechanical property controllability, topology-driven mechanical and physical property, and repeating its pattern in three-dimensional (3D) space. These properties make it extremely promising for a wide range of advanced applications. Indeed, since its first introduction, TPMSs have been applied in broad engineering sectors, such as aerospace, biomedical, sound absorbers, energy absorbing devices, and the like. As a result, TPMS architectures attract intensive research in various fields. In this regard, Zhang et al. [23] experimentally studied the energy absorption of TPMS lattices under compression load and pointed out that TPMS lattices exhibit a superior stiffness and energy absorption capability over the body-centered cubic lattices. Viet et al. [24] studied bone implants using TPMS lattice and reported that the architected implant can be an ideal candidate for bone implants. Because it provides excellent conditions for bone cell development, and significant reduction of stiffness mismatch between surrounding bone cells and implant, and becomes stiffer with increasing bone in-growth depth. Sychov et al.[25] explored the energy absorption capability of TPMSs with PLA base material and reported better energy absorption performance than conventional honeycomb in the form of a shock-absorbing layer subjected to the same conditions. Zhu et al.[26] numerically pointed out that TPMS implants with Primitive performed better in disseminating stresses within the knee joint than available conventional implant materials.

Tailoring UHPC with TPMS lattice can lead to novel superior construction materials for civil engineering applications, inheriting a hybrid of outstanding mechanical and physical properties from both TPMS lattices and UHPC. They include ultra-lightweight material but extremely high durability with corrosion and impact resistance, self-healing capability, strength controllability owing to the topology-driven property of TPMS lattice, high strength-to-weight ratio, and excellent energy absorption capability. Recently, a successful fabrication of a conventional cementitious TPMS structure with Gyroid has been presented by Nguyen et al. [27], setting a new landmark for the possible fabrication of construction materials with TPMS lattice, such as UHPC material with the TPMS lattice. However, the mechanical information of the UHPC-based TPMS lattice and UHPC-based IPCs with TPMS core is still not explored in the literature. Thus, in the present study, the anisotropy of Young's modulus and shear modulus, directional impact phase wave propagation characteristics, buckling resistance capability, and free vibration of UHPC-based TPMS lattice and steel-UHPC IPCs with TPMS cores, with a broad range of TPMS lattices, are studied. The present study provides in-depth mechanical information on such structures and assists the subsequent design and fabrication prior to their applications in civil engineering.

2. NUMERICAL APPROACHES

2.1. 3D FEM and homogenization technique

In the numerical model, the UHPC-based sheet and solid TPMS lattices, and IPCs, which contain steel TPMS core and UHPC matrix, are simulated using the commercial software Abaqus, with a broad range of TPMS topology considered, including Primitive, Gyroid, Diamond, and I-WP. The geometry of TPMS lattices in a standard tessellation language (STL) file is generated using free software, MD-TPMS [28] and subsequently sent to Abaqus for simulations. The examples of the topological configuration of the unit cell designs of UHPC-based sheet TPMS lattices and UHPC-steel IPCs with sheet TPMS core in Abaqus environment are schematically shown in Figure 1.

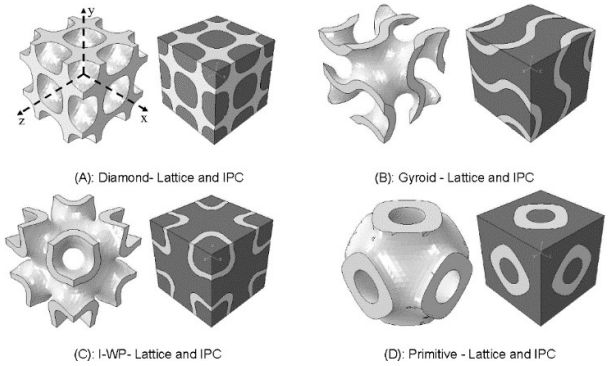

FIGURE 1. SCHEMATIC DEPICTION OF TPMS LATTICES AND IPCS IN 3D FEM SIMULATION. (A): DIAMOND TOPOLOGY; (B): GYROID TOPOLOGY; (C): I-WP TOPOLOGY; (D): PRIMITIVE TOPOLOGY.

The material properties of UHPC used in numerical simulation are obtained from well-known experimental work [29], with Young's modulus of 53.7 GPa and adopted Poisson's ratio of 0.3, and the based material, steel adopted in simulation has Young's modulus of 200 GPa and Poisson's ratio of 0.3. UHPC is assumed as an isotropic material. The Primitive lattice, I-WP lattice, Gyroid lattice, and Diamond lattice possess the trigonometrically mathematic function of the surface from Eqs. (1), (2), (3), and (4), respectively as

$$\cos(X) + \cos(Y) + \cos(Z) = c \quad (1)$$

$$2(\cos(X)\cos(Y) + \cos(Y)\cos(Z) + \cos(Z)\cos(X)) - (\cos(2X) + \cos(2Y) + \cos(2Z)) = c \quad (2)$$

$$\sin(X)\cos(Y) + \sin(Y)\cos(Z) + \sin(Z)\cos(X) = c \quad (3)$$

$$\cos(X)\cos(Y)\cos(Z) - \sin(X)\sin(Y)\sin(Z) = c \quad (4)$$

The variables are formulated as $X = 2\alpha\pi x$, $Y = 2\beta\pi y$, $Z = 2\gamma\pi z$ with α, β and γ are constant; and c can be a constant or a function, controlling the value and functional change of the solid density of porous TPMS scaffold, ry. The solid density is defined as a ratio of the volume of the solid cell of the TPMS lattice to the entire volume of structure for both cases, lattice, and IPC. It is worthwhile noting that each considered TPMS topology possesses its own unique property. Indeed, the Gyroid structure possesses a topology like that of bone tissue and has no reflection symmetry nor straight lines[30], with a smooth surface, uniform curvature radius, small anisotropy, and high manufacturability. Compared with other TPMSs, the topology of Primitive and Diamond lattices is simpler, so it is easier to design and

additively fabricate. Meanwhile, the I-WP structure exhibits the highest stiffness compared with most popular TPMS scaffolds, such as Gyroid, Primitive, and Diamond[31]. Due to these excellent properties, these four topologies are most frequently selected to represent TPMSs in research works[31]. In order to reduce the computational cost, we use the unit cell in simulation to explore the mechanical information of the entire structure. To do so, the periodic boundary conditions are adopted, with the periodicity of displacement between adjacent cells expressed as

$$u_i(x_i + g_i) = u_i(x_i) + \epsilon g_i, \forall x_i \chi_i \in \partial\lambda \quad (5)$$

In addition, the continuity of stress across the interface used for periodicity is

$$\tau_i(x_i + g_i) = -\tau_i(x_i) \quad (6)$$

In Eq.(6), term x_i represents the components of the position vector; g_i is the length of unit cell in the direction x_i; χ_i is the unit vector in the direction x_i; ϵ is the applied strain; $\partial\lambda$ is the boundary of unit cell, and τ_i is the surface traction normal to $\partial\lambda$. For further detail on applying periodic boundary conditions, it can refer to work[32]. For further details on applying periodic boundary conditions, it can refer to work[32]. By employing the homogenization technique, the effective mechanical properties, such as stress, strain, and the like can be computed as

$$\phi_e = \frac{1}{V}\int_V \boldsymbol{\phi}\, dV \quad (7)$$

Where terms ϕ_e, and $\boldsymbol{\phi}$ stand for the effective value of mechanical attribute and a tensor of mechanical property in a volume of an element dV, respectively. Finite element analysis is conducted within Abaqus, employing an average of 20000 quadratic tetrahedral elements (C3D10) to discretize the unit cell. All unit cells have a cubic shape with a dimension of 1mmx1mmx1mm chosen in simulations.

2.2. Computation of mechanical property

This subsection provides a concise overview of the established theories related to impact phase wave propagation in, buckling resistance of, and free vibration of beams constructed by UHPC-based TPMS lattices and UHPC-steel IPCs incorporating steel TPMS cores. The focus is on a cantilever beam configuration, consisting of either UHPC TPMSs or IPCs, with one end being free and the other end fixed. For other beams, ones can be inferred accordingly. The beams are assumed to be subjected to a common condition, including impact loads, axial buckling forces, or free vibrations, with an example of the beam with UHPC-based Primitive subjected to explosive impact load schematically demonstrated in Figure 2.

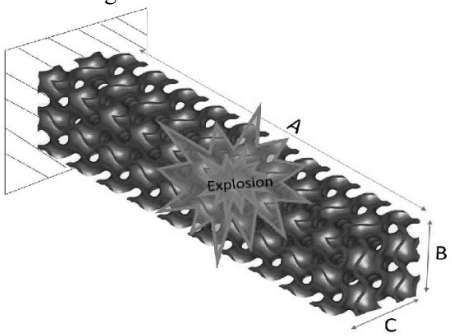

FIGURE 2. CONFIGURATION EXAMPLE OF CANTILEVER BEAM WITH UHPC GYROID SUBJECTED TO THE EXPLOSION.

Throughout the study, the beams are considered to have a length of A=2 m, height of B=0.02 m, and width of C=0.02 m.

2.2.1. Theory for the propagation of directional impact phase waves.

Investigating the impact wave propagation in UHPC IPCs with TPMSs is significant because it informs us how the IPCs respond and withstand natural and artificial harmful events, including earthquakes or explosions so that we can select the most appropriate one. Physically, faster-moving impact waves can exert high stresses in IPC-built infrastructures within a shorter period, causing more damage, including fracture, crack, and deformation. Thus, this work explores the directional shear and longitudinal phase waves propagating in UHPC-based TPMSs and UHPC-steel IPCs induced by a broad external impact source, including explosion, earthquake, direct impact, and the like. Due to the cubic symmetric behavior of the UHPC-based TPMS lattices, the wave propagation possesses the same characteristic upon the different axial directions, thus we examine the wave propagation through an infinitesimal element in x0y, generating the motion equation when it passes through as

$$\frac{\partial\sigma_{xx}}{\partial x} + \frac{\partial\sigma_{xy}}{\partial y} = \rho\ddot{u}, and \quad \frac{\partial\sigma_{yx}}{\partial x} + \frac{\partial\sigma_{yy}}{\partial y} = \rho\ddot{v} \quad (8)$$

In Eq.(8) terms $\ddot{u}$, and $\ddot{v}$ are accelerations of small element in x-direction, and y-direction, respectively. By describing the displacement in aspects of the harmonic planar wave Ansatz, it can be written

$$u = Uexp[iwt - i(kx)] \quad (9)$$

In the equation, terms w and k are the wave frequency and components of the wave vector, respectively. Substituting Eq.(9) into Eq.(8), and after a simple mathematic manipulation, the directional shear $c_{s\theta}$ and longitudinal $c_{l\theta}$ wave velocities are as [33]

$$\begin{cases} w_{s\theta} = \sqrt{\frac{-\xi_1 - \sqrt{\mu}}{2\rho^2}} \\ w_{l\theta} = \sqrt{\frac{-\xi_1 + \sqrt{\mu}}{2\rho^2}} \end{cases} \quad (10)$$

where the notations are $\xi_1 = -(C_{11}cos^2\theta + C_{44}sin^2\theta + C_{11})\rho$, and $\xi_2 = (C_{11}cos^2\theta + C_{44}sin^2\theta) - (C_{12}cos\theta sin\theta + C_{44}cos\theta sin\theta)(C_{11}cos\theta sin\theta + C_{12}cos\theta sin\theta)$; C_{11}, C_{12}, and C_{44} are the components of the stiffness tensor of isotropic material in Voigt form, and μ is defined as $\mu = \xi_1^2 - 4\rho^2\xi_2$.

2.2.2. Buckling force

When the IPCs are used to build the structural components and systems, such as columns, beams, trusses, and so on of buildings, bridges, and other structures subjected to compressive load, buckling can occur. Hence, understanding the buckling behaviour of the considered IPCs is significant for ensuring the safety, structural stability, and cost efficiency of the civil infrastructures built by them. Considering that the cantilever beams have their free tip subjected to axial load, reaching the onset of the buckling at an axial force P_c, the moment equilibrium of the Euler–Bernoulli elastic beam can be written as

$$\frac{d^2y}{dx^2} = \frac{M}{EI} = -P_c\frac{\delta - y}{EI} \quad (11)$$

Through the expansion and a simple mathematic work of second-order differential equation (11), we obtain the trigonometrical solution as

$$y = A_1 sin(\gamma x) + A_2 cos(\gamma x) + \delta \quad (12)$$

In Eq.(12), the notation φ is defined as $\varphi = P_c/(EI)$ found by the boundary conditions of the beam, δ stands for the maximum deflection of the beam, and constants A_1 and A_2 are obtained by the boundary condition of the beam. In this work, the cantilever beam is considered, with one free end and one clamped end, with a simple mathematic work relating to the value γ, the buckling force is given

$$P_c = \frac{\pi^2 EI}{4L^2} \quad (13)$$

2.2.3. Natural vibration frequency

During the free vibration, the equation governing the motion of a small element at location x in the Euler–Bernoulli beam and time t is written as the fourth order-differential equation as:

$$EI\frac{\partial^4 u(x,t)}{\partial x^4} + \rho A_a \frac{\partial^2 u(x,t)}{\partial t^2} = 0 \quad (14)$$

Where terms $A_a, I, E,$ and ρ are the cross-sectional area, the moment of inertia of A_a, Young's modulus of the beam, and mass density, respectively of the architected beams. The function $u(x,t)$ is the transverse deflection at the axial location x and time t. By using the methods of separation of eigenfunctions and variables, the differential equation of displacement with respect to the axial position is obtained as

$$\frac{d^4 U(x)}{dx^4} - \beta^4 U(x) = 0 \quad (15)$$

Let's define $\beta = \sqrt{\frac{\omega}{\sqrt{\frac{EI}{\rho A_a}}}}$ in which ω is natural frequency, the solution of Eq.(15) is given

$$U(x) = B_1 \sin(\beta) + B_2 \cos(\beta) + B_3 \sinh(\beta) + B_4 \cosh(\beta) \quad (16)$$

In the equation, terms B_1, B_2, B_3, and B_4 are constants found based on the boundary condition of the beam. Considering the cantilever beam, the value β of the first vibration mode is determined as 1.875 and subsequently, the corresponding natural frequency is computed as $\omega = 1.875^2\sqrt{\frac{EI}{\rho A_a}}$

3. EXPERIMENTAL CONDUCTION

In order to verify the correctness of the numerical model used to explore the mechanical information of UHPC-based TPMS lattices and UHPC-steel IPCs with TPMS lattice cores, the experimental work of compressive tests on PLA-based TPMS lattices and cement-PLA IPCs with sheet PLA TPMS lattice are carried out. The topology of samples is depicted in Figure 3.

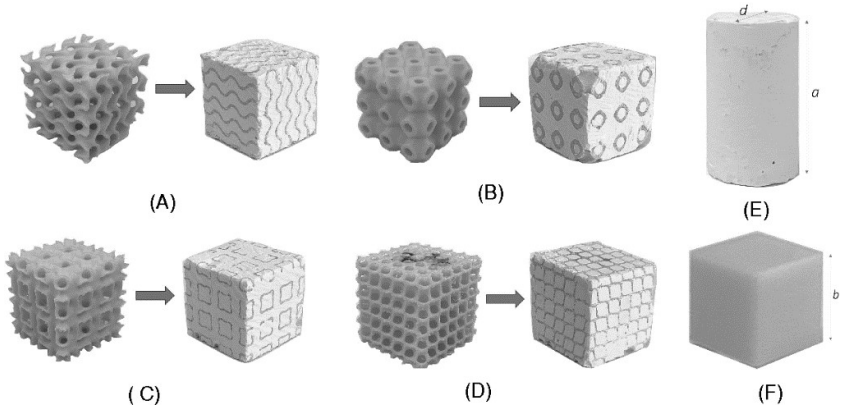

FIGURE 3. DEMONSTRATION OF EXPERIMENTAL TEST SAMPLES USED IN THIS WORK. (A): PLA SHEET GYROID LATTICE STRUCTURE AND CEMENT-PLA IPC WITH SHEET GYROID CORE; (B): PLA SHEET PRIMITIVE LATTICE STRUCTURE AND CEMENT-PLA IPC WITH SHEET PRIMITIVE CORE; (C): PLA SHEET I-WP LATTICE STRUCTURE AND CEMENT-PLA IPC WITH SHEET I-WP CORE; (D): PLA SHEET DIAMOND LATTICE STRUCTURE AND CEMENT-PLA IPC WITH SHEET DIAMOND CORE; (E): DENSE CEMENT SAMPLE; (F): DENSE PLA SAMPLE.

In the experiment, 4 samples of PLA-based TPMS structures, including sheet Gyroid, sheet Primitive, sheet Diamond, and sheet I-WP, and 4 samples of cement-PLA IPCs with PLA TPMS cores, including sheet Gyroid core, sheet Primitive core, sheet Diamond core, and sheet I-WP core are fabricated. The reason we choose PLA as the base material is that it is generally cheaper than metals, and its printing process is less expensive than that with metals, making it a popular choice to be the base material for additive printing while it accurately demonstrates the topology-driven mechanical properties of architected TPMS structures. As a result, PLA is seen to be widely used in the scientific study of the effective elastic stiffness and yield strength of TPMSs[31] and other architected materials as well. All TPMS and IPC samples have a cubic shape with a dimension of 3cmx3cmx3cm. In addition, the dense cement sample is a cylinder having a diameter d= 6mm and length a=15 mm as shown in Figure 3(E). The dense PLA sample has a cubic shape with a dimension of 1cmx1cmx1cm. The experimental fabrication of samples goes through two steps, including printing the PLAS TPMS lattices and fabricating IPCs from cement powder and PLA TPMS core. Regarding the first step, an STL file of each TPMS topology is generated and then sent to the 3D printer Ultimaker Pro to additively print the TPMS samples out. The high-quality print is set, with an infill thickness of 0.1 mm. In the second step, the printed PLA TPMS samples are dipped into a solution of cement and water, with a ratio of cement to water of 67 to 124 at room temperature. In order to make the solution fully fill the PLA

TPMS samples, the mixture is shaken with a shaking machine for 2 minutes and subsequently, the mixture is hardened at room temperature for 5 days. At the same time, the dense cement sample with the same cement-to-water ratio is also prepared, and the dense PLA cube is printed out with the same printing setup as that of TPMS samples, all depicted in Figures 1 (E) and (F). The samples are then compressively tested by the INSTRON testing machine with a load cell of 30 kN at room temperature. The test is performed by displacement control, with an incremental rate of 0.2 mm/minute and a maximum displacement of 3 mm. The stress-strain responses of samples are computed by the force-displacement responses generated by the testing machine. As a result, measured Young's modulus of dense cement and PLA samples is 0.61 GPa and 2.17 GPa, respectively. They are subsequently inputted as base materials in 3D FEM simulations using Abaqus to generate the stress-strain response of each corresponding structure subjected to compressive load and subsequently compared with the experimental result.

4. RESULTS AND DISCUSSIONS

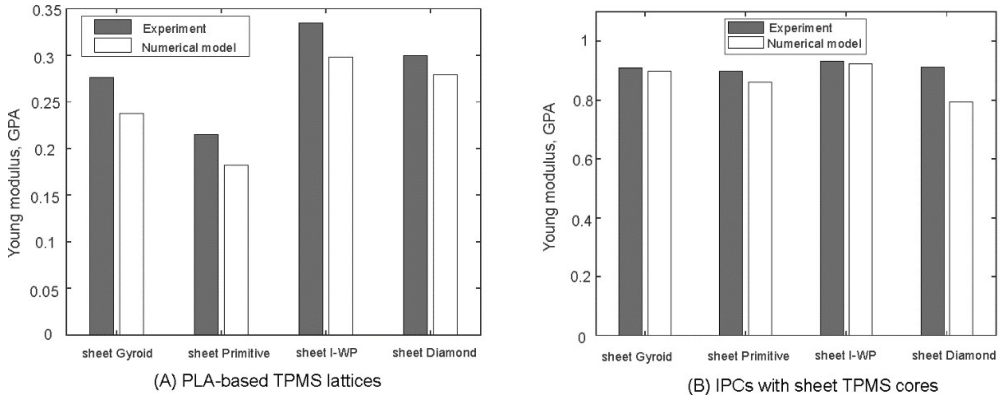

FIGURE 4. EXPERIMNETAL VALIDATION OF NUMERICAL MODEL IN TERMS OF YOUNG'S MODULUS VERSUS THE DIFFERENT TOPOLOGIES OF PLA-BASED TPMS LATTICE (A) AND CEMENT-PLA IPCS WITH TPMS CORES (B), WITH THE SOLID DENSITY BEING 0.3 FOR ALL CASES.

Figure 4 shows the experimental validation for the soundness of the numerical technique in terms of Young's modulus versus the different topologies of PLA-based TPMS lattice and cement-PLA IPCs with TPMS cores, having a solid density of 0.3 for all cases. The figure displays the fact that both prediction techniques agree with each other, where the highest percentage difference is found at approximately 15% for the cement-PLA IPC sample with sheet Diamond core and approximately 17% for the PLA sample with sheet Gyroid. These small differences prove the accuracy of the used numerical model. More specifically, Young's modulus of the PLA sample with sheet Gyroid obtained from the numerical model and experiment is 0.223 GPa and 0.27 GPa, respectively, and that of cement-PLA IPCs with sheet Diamond core obtained from the numerical and experiment is 0.92 GPa and 0.79 GPa, respectively. Additionally, both the experiment and numerical approach demonstrate a larger variation of Young's modulus among PLA TPMSs compared with that among IPCs. Therefore, IPCs can reduce the discrepancy of the mechanical properties among TPMS types driven by their unique topology.

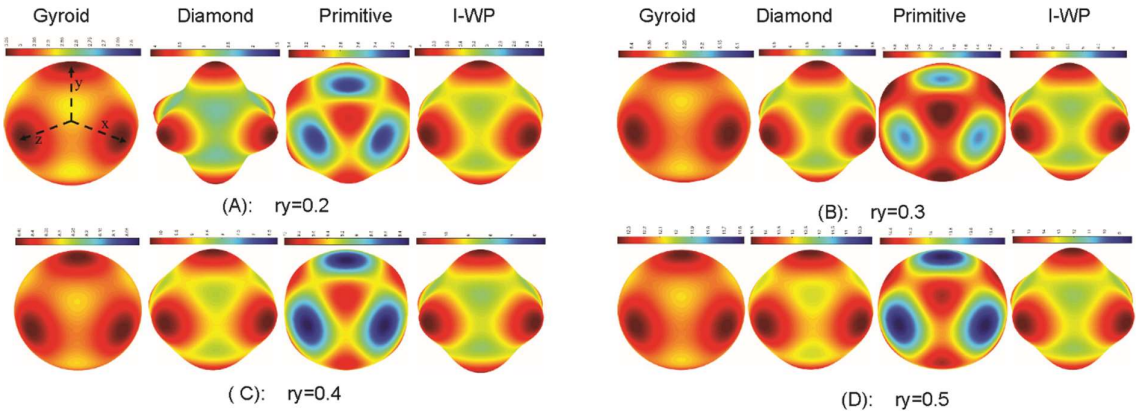

FIGURE 5. SPATIAL ANISOTROPIC SURFACE OF YOUNG'S MODULUS (GPA) OF UHPC-BASED SHEET TPMS STRUCTURES AGAINST THE VARYING ORIENTATION. (A): RY=0.2; (B): RY=0.3; (C): RY=0.4; (D): RY=0.5.

The mathematical function of anisotropic surface of Young's and shear moduli in response to the varying orientation is given

$$\vec{E} = \frac{1}{s_{11}-(2s_{11}-2s_{12}-s_{44})(j_1^2 j_2^2+j_1^2 j_3^2+j_2^2 j_3^2)} \quad (17)$$

and

$$\vec{G} = \frac{1}{s_{44}-(2s_{11}-2s_{12}-s_{44})(j_1^2 j_2^2+j_1^2 j_3^2+j_2^2 j_3^2)} \quad (18)$$

Where terms $\vec{E}$ and $\vec{G}$ are directional Young's and shear modulus, respectively; j_1, j_2, and j_3 are the directional cosines of angle between position vector of the mechanical value and axes of xyz-coordinate system; s_{11}, s_{12}, and s_{44} are elements of elastic compliance matrix in Voigt form. The spatial anisotropic surface of Young's modulus of UHPC-based sheet TPMS lattices versus the different solid densities and the varying orientation is shown in Figure 5. Generally, the figure illustrates that Young's modulus of the material demonstrates greater variability in response to varying orientation or more extreme anisotropy as material density decreases. The extreme anisotropy of Young's modulus implies that its spatial profile shape changes significantly upon the varying orientation. Interestingly, the anisotropy of the UHPC material with a sheet Gyroid displays minimal sensitivity to density variations compared to other lattices and its anisotropic level is very small and kept almost the same under the varying density, showing via the almost sphere shape. The TPMS topology can bring outstanding benefits in terms of physical and mechanical properties for UHPC-built structures, but high anisotropy requires more attention and makes the design, analysis, and fabrication more complicated when it is applied in the construction field. Hence, it can be concluded that the sheet Gyroid can be an ideal topology to fabricate UHPC-based structures in the construction field. Because it requires less care and reduces the complication of design and fabrication regardless of the variation of the solid density. Last but not least, the effective Young's modulus of UHPC material with sheet Gyroid, sheet Diamond, and sheet I-WP exhibits the highest along with the axial directions and lowest along with the diagonal directions via the origin, which is opposite to that of Primitive case. In order to observe in-depth the anisotropy of Young's modulus, its 2D surface is plotted and illustrated in Figure 6.

It is obvious evidence from the figure that the directional Young's modulus of UHPC material structured with sheet TPMSs drops with a decrease in the solid density with a nonlinear pattern. The nonlinear pattern means that the value of Young's modulus is not equally increased with an equal increase in the solid density. Particularly, Young's modulus of UHPC material with sheet Gyroid lattice in the axial direction drops from 12.3 GPa to 8.4 GPa with decreasing solid density from 0.5 to 0.4 while it drops from 5.4 GPa to 3 GPa along with decreasing solid density from 0.3 to 0.2, respectively. Moreover, the UHPC material with sheet Gyroid possesses an almost circular shape of Young's modulus against orientation regardless of the change of the solid density, meaning that it behaves nearly like isotropic material.

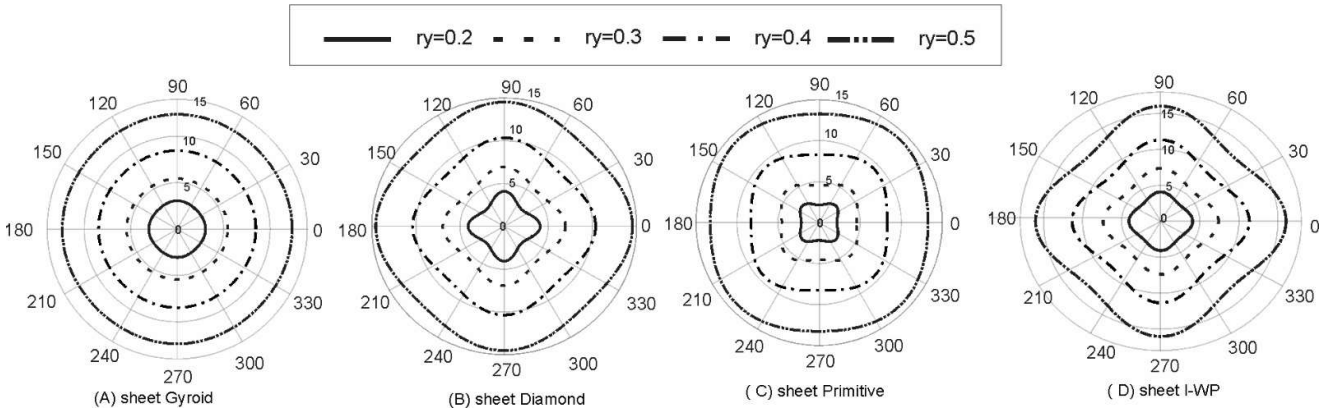

FIGURE 6. 2D SURFACE OF ANISOTROPY OF YOUNG'S MODULUS OF UHPC-BASED SHEET TPMS LATTICES AGAINST VARYING SOLID DENSITY. (A): SHEET GYROID; (B): SHEET DIAMOND; (C): SHEET PRIMITIVE; (D): SHEET I-WP.

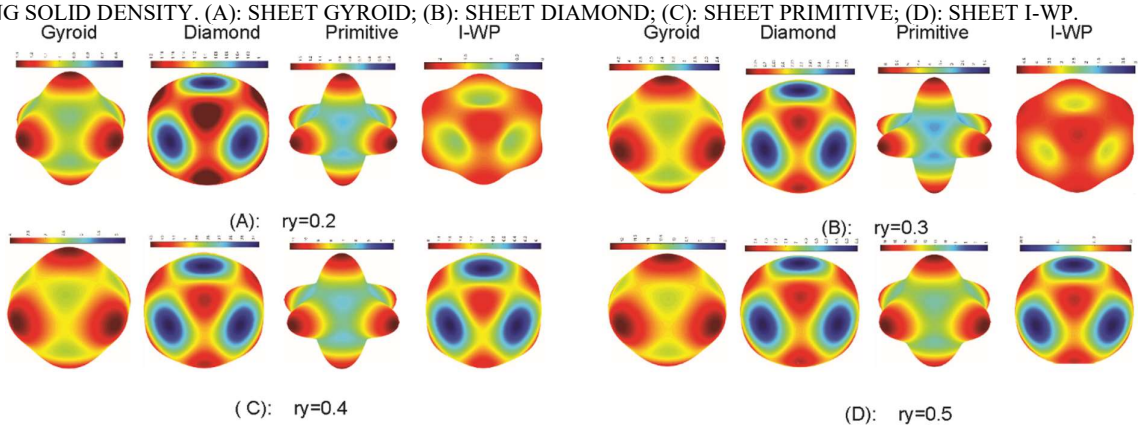

FIGURE 7. SPATIAL ANISOTROPIC SURFACE OF YOUNG'S MODULUS (GPA) OF UHPC-BASED SOLID TPMS LATTICES WITH DIFFERENT SOLID DENSITIES. (A): ry=0.2; (B): ry=0.3; (C): ry=0.4; (D): ry=0.5.

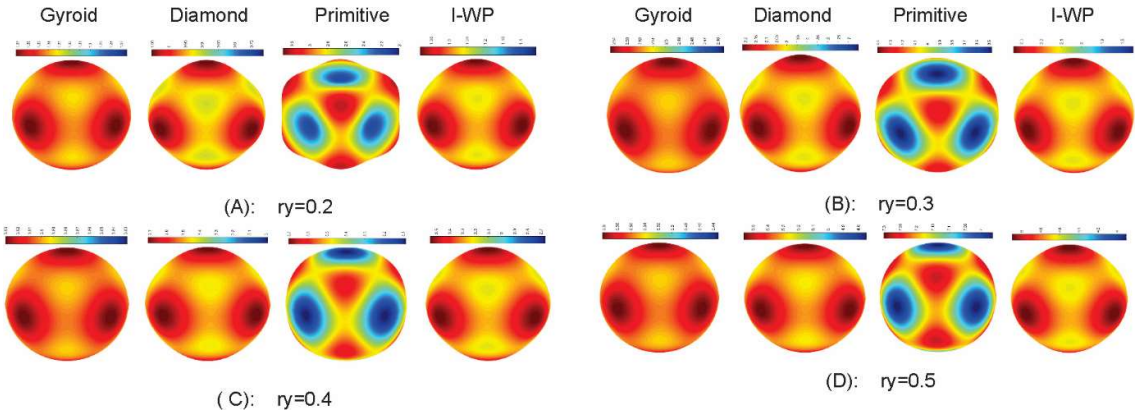

FIGURE 8. SPATIAL ANISOTROPIC SURFACE OF SHEAR MODULUS (GPA) OF UHPC-BASED SHEET TPMS LATTICES AT DIFFERENT SOLID DENSITIES. (A): ry=0.2; (B): ry=0.3; (C): ry=0.4; (D): ry=0.5.

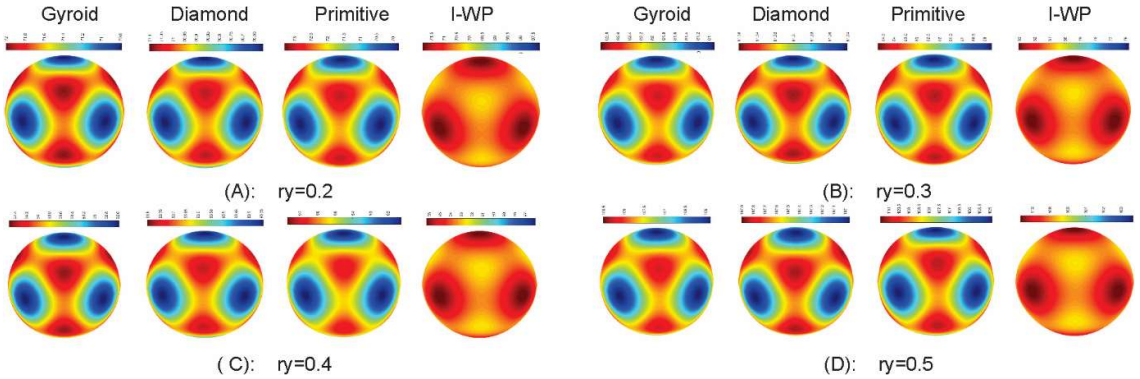

FIGURE 9. 3D ANISOTROPY OF EFFETCIVE YOUNG'S MODULUS (GPA) OF UHPC-STEEL IPCS WITH SHEET TPMS CORES. (A): ry=0.2;(B): ry=0.3; (C): ry=0.4; (D): ry=0.5.

Figure 7 illustrates the spatial anisotropic surface of Young's modulus of UHPC material structured with solid TPMS lattices with varying solid density. In particular, it can be seen from the figure that, the spatial surface of anisotropy of UHPC-based solid TPMSs is similar to that of UHPC-based sheet TPMSs, but more extreme, reflecting via the more distorted spatial surface of Young's modulus, considering both have the same solid density. Thus, the UHPC material with sheet TPMS lattice is concluded to be preferable to that of solid type at the same solid density when considered as the constructional material.

Figure 8 demonstrates the spatial anisotropic surfaces of the shear modulus of UHPC material with sheet TPMS lattices with respect to varying solid density. We can see from the figure that the anisotropy of shear modulus behaves similarly to that of Young's modulus regarding the same topology, with a more extreme upon the decreasing relative density. Also, the UHPC material with sheet Gyroid exhibits the smallest anisotropy of shear modulus among others. The shear modulus decreases with decreasing solid density, meaning that the UHPC with TPMS lattices resists the transverse deformation weaker with lower solid density.

Figure 9 depicts the 3D anisotropy of Young's modulus of UHPC-steel IPCs with sheet TPMS cores against the varying solid density, ry. The figure shows an interesting result of anisotropy of Young's modulus of IPCs that, opposite to that of UHPC material with TPMS lattice, anisotropy of IPCs is less extreme or less distorted in response to the varying orientation. It is not affected by the change of relative density or topology, significantly reducing the care and complication in analysis, design, and fabrication while maintaining low maintenance costs for the construction material. More importantly, at the same solid density, the magnitude of Young's modulus of all considered IPCs is observed to be almost the same unaffected by the change of the topology, manifesting via less discrepancy of Young's modulus. To support further the observation of anisotropy of Young's modulus of IPCs, the 2D profile of anisotropy of Young's modulus of UHPC-steel IPCs with TPMSs versus different solid density is shown in Figure 10.

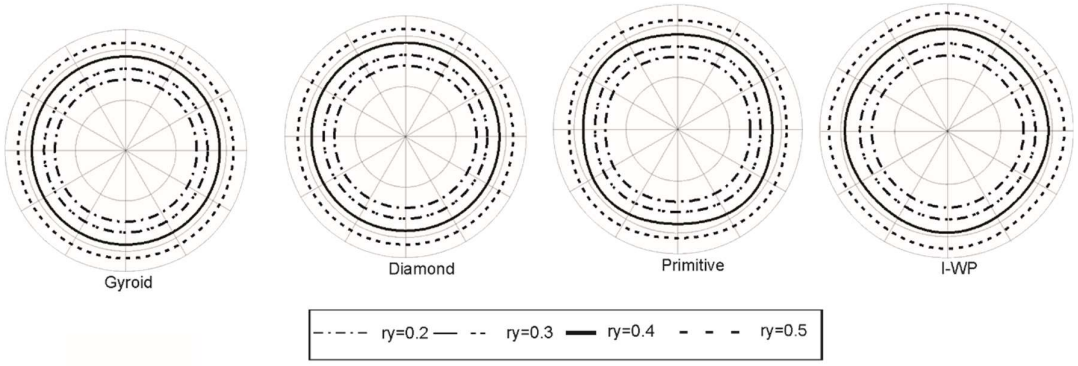

FIGURE 10. 2D ANISOTROPY PROFILE OF YOUNG'S MODULUS IN (GPA) OF IPCS.

Figure 10 shows the 2D profile of the anisotropy of Young's modulus of IPCs with respect to the changing directions. It is obvious from the figure that Young's modulus has a directional profile almost circle unaffected by the change of the solid density and TPMS topology, reflecting near-isotropic properties of UHPC-steel IPCs. Moreover, Young's modulus of UHPC material with TPMS lattices nonlinearly drops with a reduction of solid density. Among considered materials, generally, the IPC with sheet I-WP cores possesses the highest value of Young's modulus, and IPCs with sheet Primitive cores have the lowest Young's modulus, at a typical solid density. Specifically, at a solid density of 0.5, the Young's modulus of UHPC-steel IPCs with I-WP core, Gyroid core, Diamond core, and Primitive core are 117 GPa, 108 GPa, 109 GPa, and 105 GPa, respectively. This unique characteristic offers no care of a selection of TPMS lattice to make IPCs, as long as such TPMS lattice provides the ultimate mechanical performance, such as stiffness for structure compared with other TPMS lattices under the same conditions.

Figure 11 shows a comparison between steel-UHPC IPCs with sheet TPMSs and with other architected metamaterials, including spinodal structure with ry=0.3 and Menger sponge fractal with ry=0.4 in terms of effective elastic shear modulus in the yx-direction and Young's moduli in the y-direction under the same solid density and boundary conditions. In the figure, the spinodal topology is attained from the literature [34], and the Menger sponge architecture is created by merging and cutting the geometry in the Abaqus environment. Based on the figure, the UHPC IPCs with the spinodal architecture possess a higher effective shear modulus or Young's modulus than the UHPC IPCs with Primitive, Gyroid, and I-WP topologies but have a lower effective shear modulus or Young's modulus than that with the I-WP scaffold. Meanwhile, the UHPC IPCs with the Menger sponge fractal exhibit a higher effective shear modulus or Young's modulus compared to that of the UHPC IPCs with considered TPMS topologies. It is worthwhile noting that, based on our observation, although the IPCs with the Menger sponge fractal own the highest effective stiffness, its anisotropy of stiffness versus the varying orientation is more extreme than others, exhibiting a weaker response to multiaxial loads. Hence, each IPC with the architected material has its own advantage in a typical civil engineering application, which needs to be addressed before being used in the construction of the infrastructures.

To observe the anisotropy in more detail, we quantify the anisotropy of Young's modulus of UHPC material with sheet and solid TPMSs, and IPCs in aspects of a dimensionless number, Zener ratio, and then depict it in Figure 12. Knowing that the isotropy corresponds to a Zener ratio of 1, we can see that IPCs have a Zener ratio closer to 1 or much less anisotropy compared with that of UHPC material with solid and sheet TPMSs regarding the same topology and solid density. Furthermore, among UHPC-based TPMS lattices, the one with sheet Gyroid possesses a ratio close to 1. Indeed, at solid density ry=0.3, the Zener ratio of UHPC structures with sheet and solid Gyroid, sheet and solid Primitive, sheet and solid Diamond, and sheet and solid I-WP is 0.96 and 0.7, 1.5 and 0.33, 0.65 and 1.4, and 0.65 and 2.2, respectively.

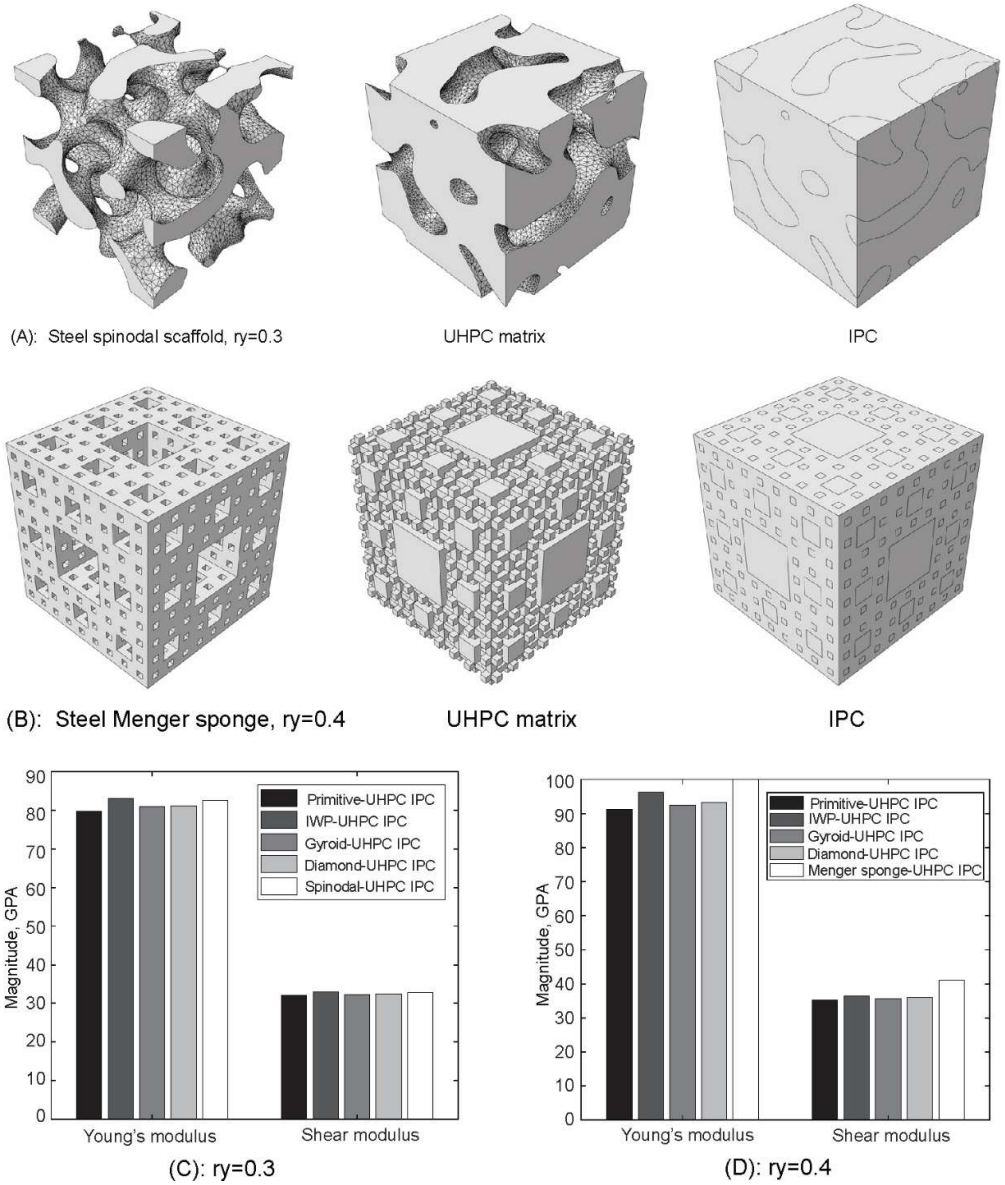

FIGURE 11. A COMPARATIVE STUDY BETWEEN UHPC IPCS WITH SHEET TPMSS AND WITH OTHER ARCHITECTED METAMATERIALS, INCLUDING SPINODAL AND MENGER SPONGE ARCHITECTURES IN TERMS OF ELASTIC SHEAR MODULUS IN THE YX-DIRECTION AND YOUNG'S MODULI IN THE Y-DIRECTION UNDER THE SAME SOLID DENSITY AND BOUNDARY CONDITIONS. (A): STEEL-UHPC IPC WITH SPINODAL ARCHITECTURE; (B): STEEL-UHPC IPC WITH MENGER SPONGE ARCHITECTURE; (C): ry=0.3; AND (D): ry=0.4.

Figure 13 shows the directional shear(SW) and longitudinal(LW) phase wave velocity propagating in UHPC-based beams with sheet TPMSs, displaying a drop in phase wave velocity with respect to the decreasing solid density in a nonlinear mode. For instance, when the solid density reduces from 0.5 to 0.2, the longitudinal wave velocity of the UHPC-based beam with sheet Primitive drops from 0.1 km/s to 0.065 km/s. Moreover, each beam is observed to possess a distinct wave propagation shape against the orientation, meaning that the anisotropy of wave propagation in the beam is unique with each UHPC lattice. Indeed, the 2D shape of both shear and longitudinal wave velocities versus the propagating direction is seen to have the biggest to smallest variation corresponding to the beam with sheet Gyroid, sheet I-WP, sheet Diamond, and sheet Primitive, respectively. Wherein, the UHPC-based beam with sheet Gyroid owns an almost round profile of wave velocity, meaning that it has the least extreme anisotropy of wave propagation and proving it as the most preferable lattice candidate for construction material in aspects of resisting the impact compared among considered TPMSs. Also, the lower solid density results in a more distorted profile of wave propagation. Last but not least, the longitudinal wave propagation in UHPC-based beam with sheet TPMSs, including Gyroid, Diamond, and I-WP is observed to be the highest in the axial direction and the lowest in the diagonal direction, which is opposite to the beam with sheet Primitive. The higher wave velocity carries a higher destructive energy; hence, rotating the direction of TPMS unit cells when applying it in building materials for the lowest impact phase wave velocity is highly recommended. Thus,

the UHPC structure with sheet Gyroid offers a great benefit for the design and fabrication of structural building materials as it does not require the rotation of the unit cell's direction for the lowest impact wave velocity, which is due to its least extreme anisotropy.

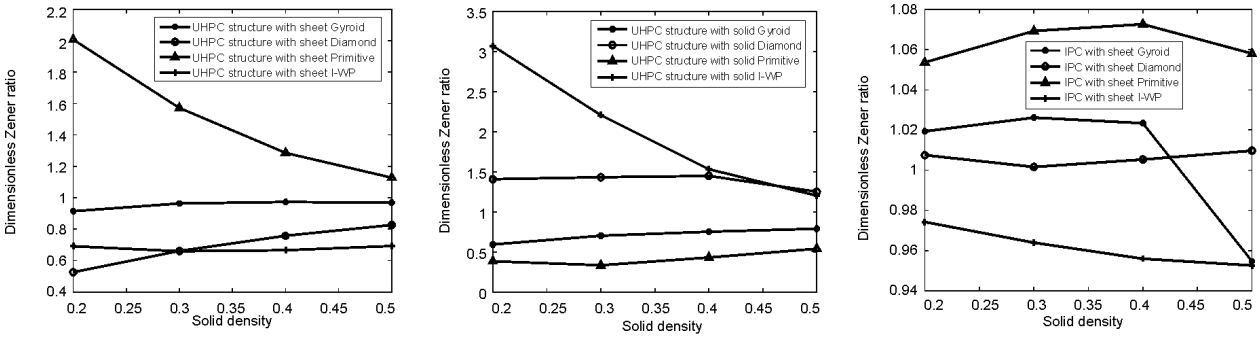

(A) UHPC-based sheet TPMS lattices (B) UHPC-based solid TPMS lattices (C) IPCs with sheet TPMS core

FIGURE 12. ZENER RATIO OF UHPC-BASED TPMS LATTICES AND IPC WITH TPMS CORES VERSUS THE SOLID DENSITY.

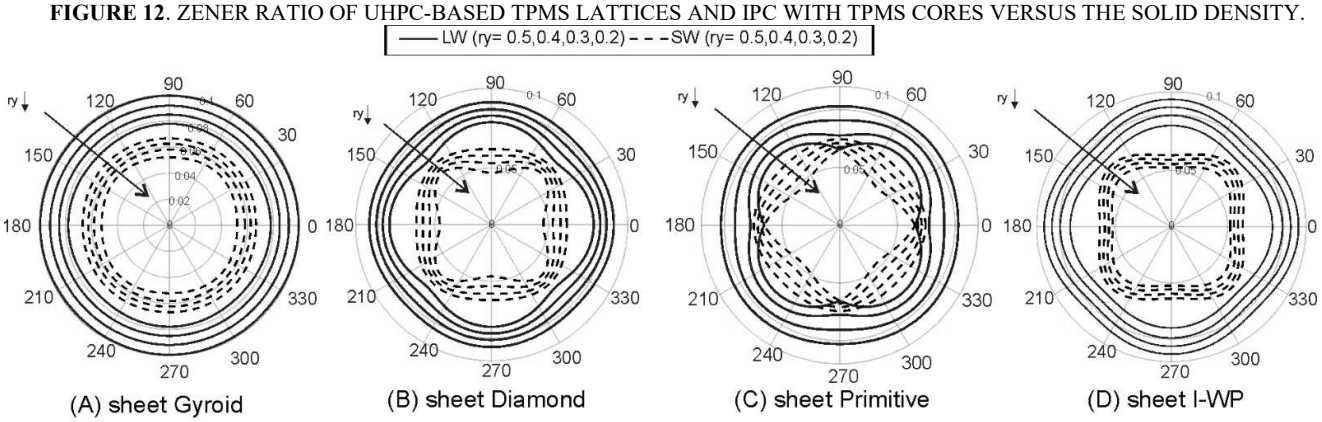

(A) sheet Gyroid (B) sheet Diamond (C) sheet Primitive (D) sheet I-WP

FIGURE 13. DIRECTIONAL SHEAR AND LONGITUDINAL LONG-FREQUENCY IMPACT PHASE WAVE VELOCITY (KM/S) PROPAGATING IN UHPC-BASED SHEET TPMS BEAMS.

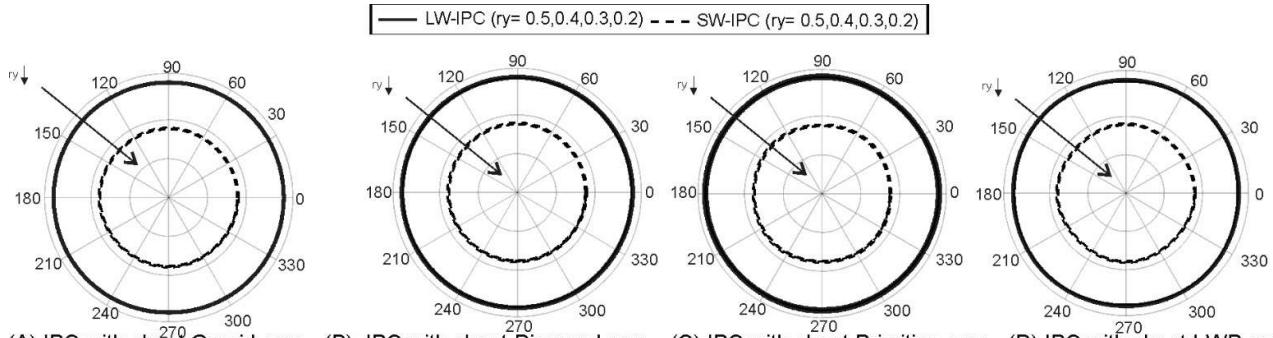

(A) IPC with sheet Gyroid core (B) IPC with sheet Diamond core (C) IPC with sheet Primitive core (D) IPC with sheet I-WP core

FIGURE 14. DIRECTIONAL SHEAR AND LONGITUDINAL PHASE WAVE PROPAGATION VELOCITY (KM/S) IN UHPC-STEEL IPCS WITH SHEET TPMS CORES.

Figure 14 shows the directional shear and longitudinal long-frequency phase wave velocity propagating in UHPC-steel IPCs with sheet TPMS cores. The results show a uniform or a closely perfect round shape of wave propagation against the varying directions, meaning that IPCs possess extremely small anisotropy in wave propagation regardless of the change of TPMS topology. Interestingly, increasing the solid density of the TPMS core and changing the topology of TPMS cores don't affect the shear or longitudinal wave velocity properties in aspects of magnitude and directional profile shape, resulting in an advantage of IPC over UHPC materials with TPMSs at the same solid density. For example, when the solid density of Primitive core drops from 0.5 to 0.2, the shear or longitudinal wave velocities propagating in the IPC beam are almost the same at 0.091 km/s or 0.148 km/s, respectively. This is due to the lesser discrepancy of mechanical properties of steel and UHPC in IPCs. We can conclude that changing the topology and solid density of TPMS cores does not affect the anisotropy of wave propagating in steel-UHPC IPCs, giving a free choice of TPMS lattice, without care of topology and solid density, when making such IPCs.

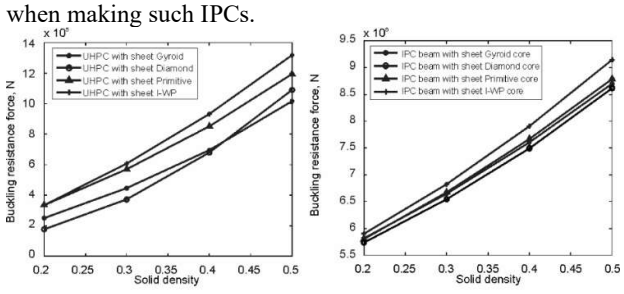

FIGURE 15. BUCKLING RESISTANCE FORCE VERSUS THE SOLID DENSITY. (A): UHPC-BASED CANTILEVER BEAM WITH SHEET TPMSS; (B): IPC-BASED CANTILEVER BEAM.

Figure 15 illustrates the buckling resistance force versus varying solid density of the UHPC-based cantilever beam with sheet TPMS lattice and IPC-based cantilever beam. From the figure, the beams resist the buckling better with a rise of solid density in a nonlinear pattern. In addition, when the solid density increases from 0.2 to 0.5, the range of buckling force of the UHPC-based beam is seen wider than that of the IPC-based beam, reflecting less influence of solid density on the buckling resistance of the IPC-beam compared with that of UHPC beam. For instance, the buckling resistance force of the UHPC beam with Gyroid lattice and the IPC beam with Gyroid core increases from 2.5 10^5 N to 10.1 10^5 N and from 5.8 10^6 N to 8.7 10^6 N, respectively when the solid density rises from 0.2 to 0.5. This is due to the fact that the IPCs contain two phases, which have a smaller discrepancy of mechanical properties between individual phases than that of the UHPC beam containing only void and UHPC. Moreover, generally among the considered TPMS geometries, the beams resist the buckling best with sheet IWP and lowest with the sheet Primitive. Although, I-WP topology provides the highest buckling resistance force, by referring to its anisotropy, rotation of the unit cell's direction is a must to have the highest buckling resistance force.

Figure 16 demonstrates the natural vibration frequency in response to varying solid density of the cantilever beam with UHPC TPMSs and IPCs. It can be seen from the figure that the two beams vibrate at a higher frequency with a rise of the solid density in an almost linear pattern. Similar to the observation of buckling force, the change of solid density leads to a wider variation of the vibrational frequency of the UHPC TPMS beam compared with that of the IPC beam. The range of vibrational frequency of the UHPC-based beam with TPMS lattice is seen as broader than that of the IPC-based beam. In particular, the UHPC-based and IPC-based beams with Gyroid vibrate at frequencies from 19.8 Hz to 40 Hz and from 36 Hz to 44 Hz, corresponding to solid density from 0.2 to 0.5, respectively. A similar explanation to buckling force can be made that the material property of the IPC beam is more homogenous than that of the UHPC beam. Lastly, the UHPC beam with sheet Gyroid and IPC beam with sheet Gyroid core are seen vibrating at the highest frequency, and the UHPC beam with sheet Primitive, and IPC beam with sheet IWP core vibrate at the lowest frequency compared with others.

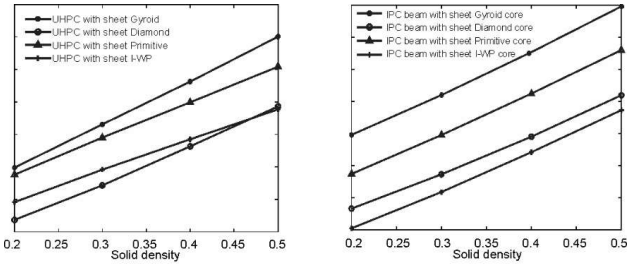

FIGURE 16. NATURAL VIBRATION FREQUENCY IN RESPONSE TO VARYING SOLID DENSITY OF CANTILEVER BEAM MADE OF (A): UHPC WITH TPMS LATTICE AND (B): IPC WITH SHEET TPMS CORE.

5. CONCLUSION

The endless improvement of additive manufacturing technology allows us to easily fabricate advanced architected metamaterial possessing outstanding topology-driven mechanical properties that cannot be found in conventional materials, ideal to be made as reinforcements for construction materials. Therefore, integrating the architected TPMSs with UHPC can produce a new type of construction material with exceptional mechanical properties. This work studies the mechanical properties of UHPC-based TPMS lattices, including sheet and solid Gyroid, Primitive, Diamond, and I-WP, and UHPC-steel IPCs with TPMS cores using numerical model and established theories. The accuracy of the numerical approach is validated by the experiment with an agreement at which the highest percent difference in aspects of Young's modulus of UHPC-based TPMS lattice is 17% realized. It can be concluded from the findings in the present study that

(i) UHPC material with sheet Gyroid has the least extreme anisotropic behaviour in response to the variation of orientation among UHPC material with other considered TPMS lattices, making it an ideal candidate for construction materials.

(ii) Compared to UHPC-based TPMS lattice, the IPCs with TPMS core possess a much smaller anisotropy and almost the same with isotropy regardless of the variation of the solid density and topology of TPMSs. Such properties

offer a free selection of TPMS lattice to make IPCs without much care of anisotropy as long as the TPMS lattice has the highest stiffness.

(iii) The UHPC IPCs with the spinodal architecture possess a higher effective shear modulus or Young's modulus than the UHPC IPCs with Primitive, Gyroid, and I-WP topologies but have a lower effective shear modulus or Young's modulus than that with the I-WP scaffold. The Menger sponge fractal exhibits a higher effective shear modulus or Young's modulus than that of the UHPC IPCs with considered TPMS topologies.

(iv) In terms of impact phase wave propagation, the impact phase wave velocity propagating in UHPC-based TPMS lattices and IPCs with TPMS cores nonlinearly drops with decreasing solid density. And, the UHPC lattice with sheet Gyroid and IPC with sheet Gyroid are found to possess the lowest phase wave velocity and exhibit the least anisotropy of wave propagation, reflecting that sheet Gyroid is an ideal candidate for UHPC-based construction material to suppress the destructive energy generated by the external impact.

(v) Bucking force decreases with dropping solid density in a nonlinear function. In all considered TPMS lattices, UHPC and IPC with sheet I-WP possess the highest buckling resistance force, however, due to the large anisotropy of UHPC lattice with I-WP, not IPCs, the attention on rotating the direction of its unit cell is required when we apply it to building materials.

(vi) The natural frequency of the UHPC beam and IPC beam show a linear drop with decreasing solid density of TPMSs, with a broader variation of frequency of the UHPC-based beam compared to that of the IPC-based beam.

The present study explores the mechanical properties of UHPC IPCs with TPMS architectures using mainly numerical models, which is its limitation and needs to be improved by performing experimental investigations for buckling behaviour, wave propagation characteristics, and free vibration property. Thus, these experimental works should be addressed in future works before implementing the material into practical application. Besides, it is worth investigating the flaw-tolerance capability of the UHPC IPCs with TPMSs in future research because the TPMS component is known for tolerating the flaw. The proposed UHPC IPCs with TPMSs can be an ideal construction material for building civil infrastructures where a high strength-to-weight ratio, small anisotropy, and corrosion and impact resistance are required.

ACKNOWLEDGEMENTS

This research is funded by University of Transport and Communications (UTC) under grant number T2024-CT-029.

REFERENCES

[1] Yao, Y., Silva, F. A., Butler, M., Mechtcherine, V., and Mobasher, B., 2021, "Tensile and Flexural Behavior of Ultra-High Performance Concrete (UHPC) under Impact Loading, " International Journal of Impact Engineering, 153, pp. 103866.

[2] Vu, T. S., Tran, B. V., Nguyen, H. Q., and Chateau, X., 2023, "A refined Morphological Representative Pattern approach to the behavior of polydisperse highly-filled inclusion–matrix composites, " International Journal of Solids and Structures, 270, pp. 112253.

[3] Le, B. A., Vu, V. H., Seo, S. Y., Tran, B. V., Nguyen-Sy, T., Le, M. C., and Vu, T. S., 2022, "Predicting the compressive strength and the effective porosity of pervious concrete using machine learning methods," KSCE Journal of Civil Engineering, 26 (11), pp. 4664-4679.

[4] Nguyen, H. Q., Tran, B. V., Vu, and T. S., 2022, "Numerical approach to predict the flexural damage behavior of pervious concrete, " Case Studies in Construction Materials, 16, pp. e00946.

[5] Vu, V. H., Tran, B. V., Le, B. A., and Nguyen, H. Q., 2021, "Prediction of the relationship between strength and porosity of pervious concrete: A micromechanical investigation," Mechanics Research Communications, 118, pp. 103791.

[6] Xi, B., Huang, Z., Al-Obaidi, S., and Ferrara, L., 2023, "Predicting ultra high-performance concrete self-healing performance using hybrid models based on metaheuristic optimization techniques, " Construction and Building Materials, 381, pp. 131261.

[7] Yoo, D. Y ., and Shin, W., 2021, "Improvement of fiber corrosion resistance of ultra-high-performance concrete by means of crack width control and repair," Cement and Concrete Composites, 121, pp. 104073.

[8] Wu, C., Oehlers, D. J., Rebentrost, M., Leach, J., and Whittaker, A. S., 2009, "Blast testing of ultra-high performance fibre and FRP-retrofitted concrete slabs," Engineering Structures, 31, pp. 2060-2069.

[9] Wu, H., Fang, Q., Chen, X. W., Gong, Z. M., and Liu, J. Z., 2015, "Projectile penetration of ultra-high performance cement based composites at 510–1320m/s," Construction and Building Materials, 74, pp. 188-200.

[10] Andrade, C., and Torres, J., 2013, "Long term carbonation of UHPC. In Proceedings of the Proceedings of International Symposium on Ultra-High Performance Fiber-Reinforced Concrete," Marseille, France, 1–3 October.

[11] Xue, J., Briseghella, B., Huang, F., Nuti, C., Tabatabai, H., and Chen, B., 2020, "Review of ultra-high performance concrete and its application in bridge engineering," Construction and Building Materials, 260, pp. 119844.

[12] Li, J., Wu, Z., Shi, C., Yuan, Q., and Zhang, Z., 2020, "Durability of ultra-high performance concrete—A review," Construction and Building Materials, 255, pp. 119296.

[13] Wu, C., Li, J., and Su, Y. D., 2018, "Development of Ultra-High Performance Concrete against Blasts: From Materials to Structures," Woodhead Publishing: Sawston, UK.

[14] Lin, T. H., Chang, C. T., Yang, B. H., Hung, C. C., and Wen, K. W., 2023, "AI-powered shotcrete robot for enhancing structural integrity using ultra-high performance concrete and visual recognition," Automation in Construction, 155, pp. 105038.

[15] Leone, M. F., and Nocerino, G., 2021, "Advanced modelling and digital manufacturing: Parametric design tools for the optimization of UHPFRC (ultra high-performance Fiber reinforced concrete) shading panels," Automation in Construction, 126, pp. 103650.

[16] Wei, J., Li, J., Liu, Z., Wu, C., and Liu, J., 2023, "Behaviour of hybrid polypropylene and steel fibre

reinforced ultra-high performance concrete beams against single and repeated impact loading," Structures, 55, pp. 324-337.

[17] Xu, J. P., Wang, Z. G., Cheng, Y. H., Wu, H., 2023, "Blast resistance of ultra high performance concrete-filled steel tube (UHPC-FST) pier against vehicular bombs," Thin-Walled Structures, 190, pp. 110990.

[18] Mirdan, D., and Saleh, A. R., 2022, "Flexural performance of reinforced concrete (RC) beam strengthened by UHPC layer," Case Studies in Construction Materials, 17, pp. e01655.

[19] Zhang, Y., Li, X., Zhu, Y., and Shao, X., 2020, "Experimental study on flexural behavior of damaged reinforced concrete (RC) beam strengthened by toughness-improved ultra-high performance concrete (UHPC) layer," Composites Part B: Engineering, 186, pp. 107834.

[20] Zhang, Y., Zhu, Y., Qiu, J., Hou, C., and Huang, J., 2023, "Impact of reinforcing ratio and fiber volume on flexural hardening behavior of steel reinforced UHPC beams," Engineering Structures, 285, pp. 116067.

[21] Yu, J., Liang, S. L., Ren, Z. P., Deng, Y. J., and Fang, Q., 2023, "Structural behavior of steel-concrete-steel and steel-ultra-high-performance-concrete-steel composite panels subjected to near-field blast load," Journal of Constructional Steel Research. 210, pp. 108108.

[22] Liu, K., Wu, C., Li, X., Tao, M., Li, J., Liu, J., and Xu, S., 2022, "Fire damaged ultra-high performance concrete (UHPC) under coupled axial static and impact loading," Cement and Concrete Composites. 126, pp. 104340.

[23] Zhang, L., Feih, S., Daynes, S., Chang, S., Wang, M. Y., Wei, J., and Lu, W. F., 2028, "Energy absorption characteristics of metallic triply periodic minimal surface sheet structures under compressive loading," Additive Manufacturing, 23, pp. 505-515.

[24] Viet, N. V., Waheed, W., Alazzam, A., and Zaki, W., 2023, "Effective compressive behavior of functionally graded TPMS titanium implants with ingrown cortical or trabecular bone," Composite Structures, 303, pp. 116288.

[25] Sychov, MM., Lebedev, LA., Dyachenko, SV., and Nefedova, LA., 2018, "Mechanical properties of energy-absorbing structures with triply periodic minimal surface topology," Acta Astronautica, 150, pp. 81–84.

[26] Zhu, LY., Li, L., Li, ZA., Shi, JP., Tang, WL., Yang, JQ., and Jiang, Q. 2019, "Design and biomechanical characteristics of porous meniscal implant structures using triply periodic minimal surfaces," Journal of Translational Medicine, 17, 89.

[27] Nguyen-Van, V., Tran, P., Peng, C., Pham, L., Zhang, G., and Nguyen-Xuan, H., 2020, "Bioinspired cellular cementitious structures for prefabricated construction: Hybrid design & performance evaluations," Automation in Construction, 119, pp. 103324.

[28] Lu, C., Lesmana, L. A., Chen, F., and Aziz, M., 2023, "MD-TPMS: Multi-dimensional gradient minimal surface generator," Software Impacts, 17, pp. 100527.

[29] Cusatis, G., El-Helou, R. G., Lale, E., and Moen, C. D., 2016, "Ultra-High Performance Concrete Compression and Fracture Response Parameters for Lattice Discrete Particle Model Simulations," International Interactive Symposium on Ultra-High Performance Concrete, 1(1).

[30] Yang, E., Leary, M., Lozanovski, B., Downing, D., Mazur, M., Sarker, A., Khorasani, AM., Jones, A., Maconachie, T., Bateman, S., Easton, M., Qian, M., Choong, P., and Brandt, M. 2019, "Effect of geometry on the mechanical properties of Ti-6Al-4V Gyroid structures fabricated via SLM: A numerical study," Materials and Designs, 184, pp. 108165.

[31] Viet, NV., Karathanasopoulos, N., and Zaki, W. 2022, "Mechanical attributes and wave propagation characteristics of TPMS lattice structures," Mechanics of Materials, 172, pp. 104363.

[32] Viet, N. V., Al-Rub, R. A., and Zaki, W., 2022, "Mechanical Behavior of Shape-Memory Alloy Triply Periodic Minimal Surface Foam Based on Schwarz Primitive," Journal of Engineering Mechanics, 148(9).

[33] Viet, N. V., Alagha. R., and Zaki, W., 2023, "Directional long-frequency phase wave propagation characteristics, anisotropy, and effective yield surfaces of architected spinodal constructs," International Journal of Solids and Structures, 264, pp. 112105.

[34] Meng-Ting, H., Bianca, E., Yunfei, Z., Jens, B., and Lorenzo, V., 2019, "The mechanical response of cellular materials with spinodal topologies," Journal of the Mechanics and Physics of Solids, 125, pp. 401–419.

FIGURES LIST